Article

Discovery Medicine 2024; 36(189): 2013–2025
https://doi.org/10.24976/Discov.Med.202436189.185

Establishment of a Disease Model Using Patient-Specific Induced Pluripotent Stem Cells-Derived Trabecular Meshwork Cells in a Chinese Primary Open-Angle Glaucoma Mega-Pedigree

Huifeng Rong[1], Ziming Luo[1], Mingjun Tang[1], Jiaqi Tang[1], Kaijing Li[1], Runcai Yang[1], Zhigang Fan[1], Nannan Sun[1], Jian Ge[1,*]

[1]State Key Laboratory of Ophthalmology, Zhongshan Ophthalmic Center, Sun Yat-sen University, Guangdong Provincial Key Laboratory of Ophthalmology and Visual Science, Guangdong Provincial Clinical Research Center for Ocular Diseases, 510060 Guangzhou, Guangdong, China
*Correspondence: gejian@mail.sysu.edu.cn (Jian Ge)
Published: 20 October 2024

Background: Primary open-angle glaucoma (POAG) is one of the most common insidious blinding eye diseases. Understanding the pathogenic mechanisms of it is extremely important. It is accepted that POAG attacks specific ocular tissue, such as trabecular meshwork and optic nerve damage, which causes elevated intraocular pressure and optic nerve damage. This study aimed to develop a preliminary prediction model for this disease by establishing the patient-specific induced pluripotent stem cells (iPSCs)-derived trabecular meshwork cells (TMCs) (p-iPSCs-TMCs) in the largest POAG family named "GZ.1" in China and preliminarily analyze the pathogenic mechanisms.

Methods: Peripheral blood of patients in GZ.1 and healthy individuals not belonging to the family were collected and reprogrammed into iPSCs. Then, the iPSCs were differentiated into iPSCs-TMCs. Next, their morphology and function were compared. Finally, their pathogenic mechanisms were analyzed.

Results: The patient-specific iPSCs (p-iPSCs) and healthy individual-specific iPSCs (n-iPSCs) were all successfully generated. Their morphology was quite similar to each other. However, p-iPSCs-TMCs exhibited compromised morphology and function. p-iPSCs-TMCs displayed the morphology of heterogeneous distribution and accumulation in clusters, while n-iPSCs-derived TMCs (n-iPSCs-TMCs) showed a uniformly distributed and homogenous appearance. Moreover, p-iPSCs-TMCs showed greater cell apoptosis ($p < 0.01$), impaired proliferating ability (24-h and 48-h time points: $p < 0.05$, 72-h and 96-h time points: $p < 0.001$), production of reactive oxygen species ($p < 0.05$), and impaired phagocytosis ability than n-iPSCs-TMCs (24-h, 48-h, and 72-h time points: $p < 0.0001$, 96-h time point: $p < 0.001$).

Conclusion: The p-iPSCs-TMCs can be successfully differentiated from peripheral blood, while the cells show impaired morphology and function compared with n-iPSCs-TMCs. Given this, p-iPSCs-TMCs can serve as an ideal disease model for POAG in GZ.1. Our study on the morphology and function of iPSCs-TMCs in GZ.1 may provide a valuable tool for elucidating the pathogenesis of POAG.

Keywords: primary open-angle glaucoma; GZ.1; induced pluripotent stem cells; trabecular meshwork cells

Introduction

According to the report [1], there will be 1.1 billion glaucoma patients by 2040. Primary open-angle glaucoma (POAG), known as the thief of sight, accounts for most cases of glaucoma, which is the second leading cause of irreversible blindness worldwide. Many studies have reported that inheritance plays a very important role in the pathogenesis of POAG [2,3]. Thus, intensive research on the POAG family is critical to our understanding of the pathogenesis of this disease [4]. Induced pluripotent stem cells (iPSCs) are considered a promising research vehicle for diseases due to their ability to differentiate into organoids that effectively mimic the disease process *in vivo* [5,6]. So far, several disease models have been successfully built [7–10]. However, few cases of patient-specific iPSCs-derived trabecular meshwork cells (TMCs) (p-iPSCs-TMCs) in POAG families have been reported.

Our team has followed the largest pedigree of POAG named "GZ.1" for many years in China [11]. We have observed that as the number of family members gradually increases (from 51 to 91), many different and peculiar phenotypes appear. The details are described in our forthcoming paper. Therefore, a patient-specific disease model in GZ.1 is desperately needed to study the underlying mechanisms. This study successfully established p-iPSCs-TMCs. Then,

their morphology and function were observed and compared with the healthy individual-specific iPSCs-derived TMCs (n-iPSCs-TMCs). Studies hold that TMCs of POAG patients show abnormalities in the structure and function, with their cytoskeletal alterations and excessive accumulation of extracellular matrix (ECM), resulting in increased trabecular meshwork stiffness, decreased compliance, and increased resistance to aqueous humor outflow, leading to pathologically high intraocular pressure (IOP) [12]. Meanwhile, it has been found that the TMCs of POAG patients have increased oxidative stress accompanied by accelerated apoptosis and cellular aging, leading to their dysfunction [13]. To find out whether the p-iPSCs-TMCs have the same characteristics as those of TMCs of POAG patients, representative genes in the trabecular meshwork cytoskeleton proteins [14], ECM [15], and inflammatory and apoptotic pathway were chosen for study. In addition, functional changes in p-iPSCs-TMCs were explored through apoptosis and proliferation assays, intracellular reactive oxygen species (ROS) assays, and phagocytosis assays. Our study successfully established a disease model of POAG in GZ.1, which may set the stage for future studies of pathogenesis and the treatment of POAG in this family.

Materials and Methods

Reprogramming and Induced Pluripotent Stem Cells (iPSCs) Culture

The reprogramming was performed according to the classic protocol of StemCell [16–18]. Inclusion criteria for subjects: patients in GZ.1 and healthy individuals not from GZ.1. There were five patients and two healthy individuals not from GZ.1. Erythroid Progenitor Reprogramming Kit (StemCell Technologies, #05924, Vancouver, B.C., Canada) was used to perform the reprogramming. In brief, 4 mL of peripheral blood was collected from the subjects. Then, red blood cells, platelets, and lineage-directed cells were removed from the peripheral blood using RosetteSep Human Progenitor Cell Basic Pre-Enrichment Kit (StemCell Technologies, #15216) and SepMate Density Gradient Centrifuge Tubes (StemCell Technologies, #15410). The enriched cells were cultured in StemSpan SFEM II medium (StemCell Technologies, # 09605) mixed with StemSpan Erythroid Expansion Supplement (100×) (StemCell Technologies, # 02692) for erythroid progenitor cell expansion to generate sufficient cells. Then, the cells were reprogrammed into iPSCs by transduction of the plasmids expressing four reprogramming factors (Octamer-Binding Transcription Factor 4 (OCT4), SRY-Box Transcription Factor 2 (SOX2), KLF Transcription Factor 4 (KLF4), and MYCL Proto-Oncogene, BHLH Transcription Factor (MYCL/L-MYC)) (#27077, #27078, #27080, ADDGene, Watertown, MA, USA). Neon Transfection System (Invitrogen, #MPK5000, Carlsbad, CA, USA) was used to introduce the vectors into the cells. On the third and fifth days, the StemSpan Erythroid Expansion Supplement (StemCell Technologies, #02692) was added to the ReproTeSR medium (StemCell Technologies, #05926) to promote the adherence of transfected cells. The culture medium was changed daily until iPSC colonies were observed (21–28 days). iPSC clones were mechanically selected and expanded. Identification was carried out using the previous method [19]. iPSCs were adherent cultured in media consisting of mTeSR1 Basal Medium and mTeSR1 5× Supplement (StemCell Technologies, #85850) and passaged every 4 to 5 days on Matrigel-coated (BD Bioscience, #356234, Hackensack, NJ, USA) plates. The iPSC line from the healthy individual not belonging to the family was previously cultured in our laboratory.

Differentiation of iPSCs into Trabecular Meshwork Cells (TMCs) (iPSCs-TMCs)

Some changes to the differentiation method were made based on previous experiments [14]. Human trabecular meshwork cells (HTMCs) were purchased from ScienCell (#6590, San Diego, CA, USA). After receiving the cells, they were identified by Immunofluorescence (IF) staining for specific markers (**Supplementary Fig. 1**). The third passage to eighth passage cells were used in the experiment. No mycoplasma contamination was detected in the cells, and they were monitored by the EZ-PCR Mycoplasma Test Kit (BI, #20-700-20, Beit Haemek, Israel) (**Supplementary Fig. 2**). The culture protocol followed the instructions on the official website of ScienCell (https://sciencellonline.com/human-trabecular-meshwork-cells/). HTMCs were cultured in the six-well plate (Corning, #3335, New York, NY, USA) and passed on every one to three days. Differentiation was initiated when the culture of HTMCs was approximately 80% confluent. Before induction, the suspension of HTMCs was collected in 50 mL centrifuge tubes (Corning, #430829, New York, NY, USA) and filtered with a membrane filter (pore size 0.2 μm) (Millipore, #ISEQ00010 and SLGP033RB, Darmstadt, Germany). Then, the filtered suspension was mixed with fresh Trabecular Meshwork Cell Medium (TMCM) (1:1) (ScienCell, #6591, San Diego, CA, USA). iPSCs were adherent cultured following the above method. When the iPSC colonies were observed, the iPSC medium was removed, and the mixed medium was added to induce differentiation. The medium was changed daily until >90% of the iPSCs were differentiated into iPSCs-TMCs (4 weeks). IF staining was performed to identify the expression of TMC markers and confirm successful induction.

Immunofluorescence (IF) Staining

IF staining was performed as previously described [20]. The adherent-cultured cells were fixed in 4% paraformaldehyde (PFA) (Leagene Biotechnology, # DF0135, Beijing, China) for 15 minutes and rinsed with phosphate-buffered saline (PBS) three times. Then, the

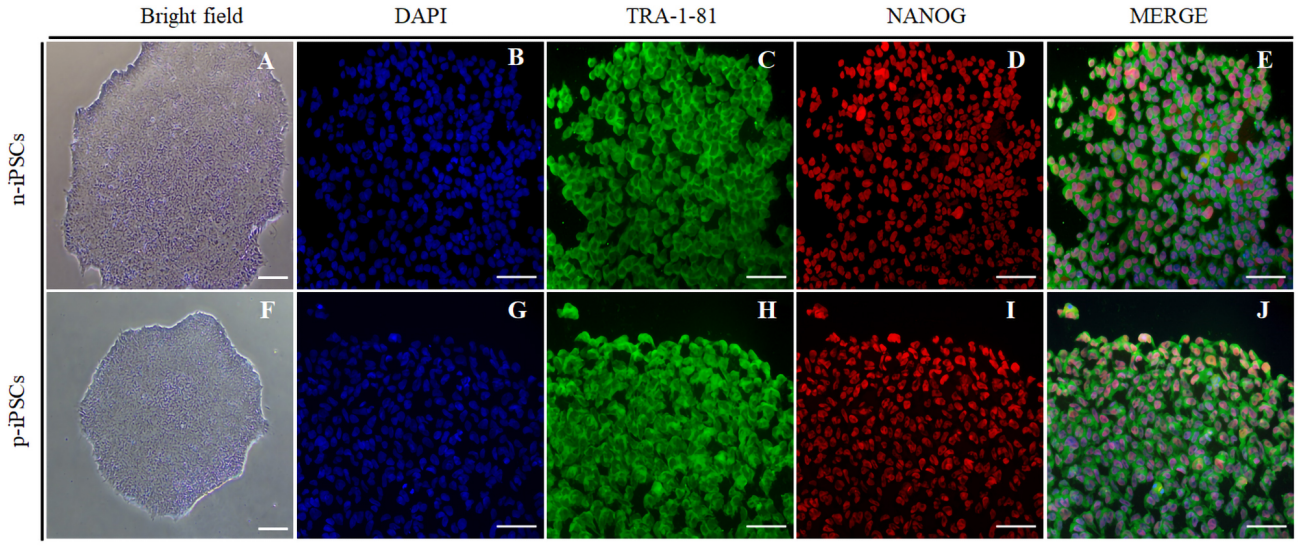

Fig. 1. Morphology and IF staining results of iPSCs' markers in n-iPSCs and p-iPSCs. (A) The typical clonal morphology of the n-iPSCs under the light microscope. (B–E) The IF staining results of the positive expression of pluripotent markers TRA1-81 and NANOG in n-iPSCs. (F) The typical clonal morphology of the p-iPSCs under the light microscope. (G–J) The IF staining results of the positive expression of pluripotent markers TRA1-81 and NANOG in p-iPSCs. A and F, scale bars, 200 μm; B–E and G–J, scale bars, 100 μm. IF, immunofluorescence; n-iPSCs, healthy individual-specific induced pluripotent stem cells; p-iPSCs, patient-specific induced pluripotent stem cells; TRA-1-81, T Cell Receptor Alpha Locus-1-81; NANOG, Nanog homeobox.

cells were permeabilized for 20 minutes with 0.25% Triton X-100 (MP Biomedicals, #0219485480, Santa Ana, CA, USA) at room temperature. PBS and permeabilizing agent (0.25% Triton X-100: donkey serum = 9:1) were prepared at 8:2 as the dilution, and the primary antibody was diluted according to the manufacturer's instructions. After blocking with donkey serum (Solarbio, #SL050, Bejing, China), cells were stained with primary antibodies against T Cell Receptor Alpha Locus-1-81 (TRA-1-81) (Abcam, #ab16289, Mouse monoclonal, Cambridge, UK), Nanog homeobox (NANOG) (Abcam, #ab21624, Rabbit polyclonal, Cambridge, UK), SOX2 (Abcam, #ab92494, Rabbit monoclonal, Cambridge, UK), Myocilin (MYOC) (Santa Cruz, #sc-20976, Mouse monoclonal, Dallas, TX, USA), Octamer-Binding Transcription Factor 4 (OCT4) (Abclonal, #A7920, Rabbit polyclonal, Wuhan, China), Vascular Cell Adhesion Molecule 1 (VCAM1) (BOSTER, #BM4289, Rabbit monoclonal, Wuhan, China), Interleukin 1 Beta (IL-1β) (Cell Signaling Technology, #CST12703, Rabbit monoclonal, Danvers, CO, USA), Tumor Necrosis Factor-alpha (TNF-α) (Cell Signaling Technology, #CST8184, Rabbit monoclonal, Danvers, CO, USA), Nuclear Factor Kappa B (NF-κB) (Cell Signaling Technology, #CST8242T, Rabbit monoclonal, Danvers, CO, USA), Caspase 3 (CASP3) (Abcam, #ab13847, Rabbit polyclonal, Cambridge, UK), TIMP metallopeptidase inhibitor 3 (TIMP3) (Abcam, #39184, Rabbit polyclonal, Cambridge, UK), Laminin Subunit Alpha 4 (LAMA4) (BOSTER, #BM1225, Mouse monoclonal, Wuhan, China), and Actin Alpha 2, Smooth Muscle (ACTA2) (Abcam, #ab119952, Mouse monoclonal, Cambridge, UK) at 4 °C overnight. The cells were incubated with a specific secondary antibody (Alexa Fluor 488 or 555 conjugated, 1:500, Thermo Fisher Scientific, #A21206, #A31572, #A21202, #A31570, Waltham, MA, USA) (diluted with the above dilution ratio according to the manufacturer's instructions) for 45 minutes at room temperature. 4′,6-Diamidino-2-phenylindole (DAPI) was used for nuclear counterstaining (Molecular Probes, #D1306, Waltham, MA, USA). Fluorescence images were acquired with a fluorescence microscope (Carl Zeiss, Axio Imager. Z2, Oberkochen, Germany). 353 nm (Excitation wavelength) and 465 nm (Emission wavelength) were used for the DAPI channel, 488 nm (Excitation wavelength) and 509 nm (Emission wavelength) were used for the green channel, and 553 nm (Excitation wavelength) and 568 nm (Emission wavelength) were used for the AF555 channel.

Quantitative Real-Time Polymerase Chain Reaction (qRT-PCR)

Total RNA isolation was performed with an RNA Quick Purification kit (Esscience, #RN001, Shanghai, China), and RNA concentration was measured by a NanoDrop 1000 spectrophotometer (Thermo Fisher Scientific, Waltham, MA, USA). First-strand complementary DNA (cDNA) was synthesized with a PrimeScript RT Master Kit (Takara Bio, #RR036A, Kusatsu, Japan) on a PTC-200 Thermal Cycler (Bio-Rad, Hercules, CA, USA) according to the manufacturer's instructions. Quantitative Real-Time Polymerase Chain Reaction (qRT-PCR) was

Table 1. The sequences of qRT-PCR primers.

Gene	Forward (5′-3′)	Reverse (5′-3′)
MYOC	ATTCTTGGGGTGGCTACACG	TGATGAAGGCATTGGCGACT
TGF-β2	CCATCCCGCCCACTTTCTAC	AGCTCAATCCGTTGTTCAGGC
FN1	AGGAAGCCGAGGTTTTAACTG	AGGACGCTCATAAGTGTCACC
VTN	AGTCCACTGAGTACCGGAGAC	CATTTCACGCATCTGGCGTTC
TIMP3	CAGGTCGCGTCTATGATGGC	AGGTGATACCGATAGTTCAGCC
ACTA2	TCAATGTCCCAGCCATGTAT	CAGCACGATGCCAGTTGT
VCAM1	AAAACAATGAGCTGAGAGGCA	TCAAGGAACTCCTCCAGTTCTC
LAMA1	GTCAGCGACTCAGAGTGTTTG	CTTGGGTGAAAGATCGTCAGC
COL4A5	CAAAAGGTGATCGTGGTTTCCC	GTCCAGGTTGTCCATTTGGTC
MMP2	GATACCCCTTTGACGGTAAGGA	CCTTCTCCCAAGGTCCATAGC
BMP4	TAGCAAGAGTGCCGTCATTCC	GCGCTCAGGATACTCAAGACC
TNC	AGGGCAAGTGCGTAAATGGAG	TGGGCAGATTTCACGGCTG
PALLD	TGAGGGAATGCCAGTAACTTTC	CTGTGGTATGGAGGGAGCA
MFAP1	AACCGCCCATTCAGTCTACG	CGGACACATAACGCTTTACCTTC
MGP	CGTTCGCAAAGTCTGTAGTCATC	CCTTCATATCCCCTCAGCAGA
CASP3	AGAACTGGACTGTGGCATTGAG	GCTTGTCGGCATACTGTTTCAG
TNF-α	GAGGCCAAGCCCTGGTATG	CGGGCCGATTGATCTCAGC
NF-κB	GGTGCGGCTCATGTTTACAG	GATGGCGTCTGATACCACGG
IL-1β	ATGATGGCTTATTACAGTGGCAA	GTCGGAGATTCGTAGCTGGA
IL-6	AATAACCACCCCTGACCCAAC	AATCTGAGGTGCCCATGCTAC
IL-8	ACTGAGAGTGATTGAGAGTGGAC	AACCCTCTGCACCCAGTTTTC
ACTB	CACCATTGGCAATGAGCGGTTC	AGGTCTTTGCGGATGTCCACGT

qRT-PCR, Quantitative Real-Time Polymerase Chain Reaction; *MYOC*, Myocilin; *TGF-β2*, Transforming Growth Factor Beta 2; *FN1*, Fibronectin 1; *VTN*, Vitronectin; *TIMP3*, TIMP metallopeptidase inhibitor 3; *ACTA2*, Actin Alpha 2, Smooth Muscle; *VCAM1*, Vascular Cell Adhesion Molecule 1; *LAMA1*, Laminin Subunit Alpha 1; *COL4A5*, Collagen Type IV Alpha 5 Chain; *MMP2*, Matrix Metallopeptidase 2; *BMP4*, Bone Morphogenetic Protein 4; *TNC*, Tenascin C; *PALLD*, Palladin; *MFAP1*, Microfibril Associated Protein 1; *MGP*, Matrix Gla Protein; *CASP3*, Caspase 3; *TNF-α*, Tumor Necrosis Factor-alpha; *NF-κB*, Nuclear Factor Kappa B; *IL-1β*, Interleukin 1 Beta; *IL-6*, Interleukin 6; *IL-8*, Interleukin 8; *ACTB*, actin beta.

performed using the LightCycler 480 SYBR Green I Master (Roche, #4887352001-1, Basel, Switzerland) on a LightCycler 480II system (Roche, Basel, Switzerland). Experiments were performed in triplicate independently. Target gene expression relative to an internal reference gene (*β*-actin (*ACTB*)) was calculated using $2^{-\Delta\Delta Ct}$. Primer sequences are listed in Table 1 (Qingke, Beijing, China).

Terminal Deoxynucleotidyl Transferase-Mediated dUTP Nick-End Labeling (TUNEL) Assay

Cell apoptosis was detected using an *in situ* cell death detection kit (Roche, #12156792910, Switzerland). Initially, fixed cells were permeabilized with a solution containing 0.1% Triton X-100 in 0.1% sodium citrate at a temperature of 4 °C for two minutes. Subsequently, the cells were washed with PBS and then incubated with the Terminal Deoxynucleotidyl Transferase-Mediated dUTP Nick-End Labeling (TUNEL) reaction mixture, which had been prepared in advance following the provided instructions, at a temperature of 37 °C in a dark environment. Following this incubation, the cells were washed with PBS three times and stained with DAPI. Images were acquired using a fluorescence microscope (Carl Zeiss, Axio Imager. Z2, Oberkochen, Germany). 353 nm (Excitation wavelength) and 465 nm (Emission wavelength) were used for the DAPI channel, and 558 nm (Excitation wavelength) and 575 nm (Emission wavelength) were used for the Rhodamine channel. The final results were determined by calculating the average number of cells in four randomly selected fields from different fluorescence channels under the microscope in each experiment. The assay was conducted independently in triplicate.

Cell Counting Kit-8 (CCK-8)

Cell viability was assessed using a Cell Counting Kit-8 (CCK-8) assay following the guidelines provided by the manufacturer (Dojindo, #CK04, Kumamoto, Japan). Briefly, cells were seeded into a 96-well plate at a density of 5000 cells per well. At 24, 48, 72, and 96 hours, 10 microliters of CCK-8 solution were added to each well. The plates were then incubated at 37 °C for one hour. Subsequently, the measurement of absorbance at a wavelength of

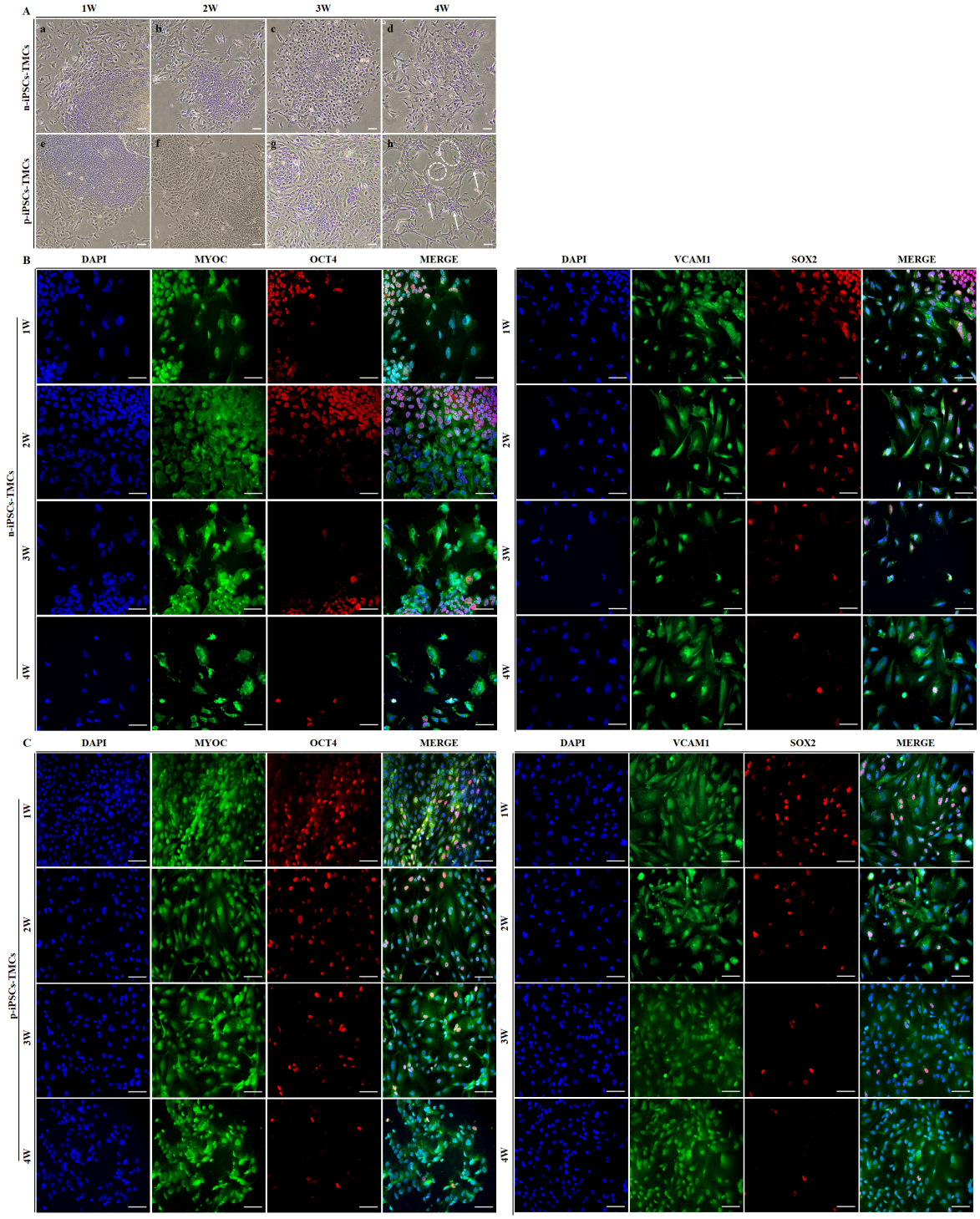

Fig. 2. The morphology and marker expression comparison of n-iPSCs-TMCs and p-iPSCs-TMCs. (A) During the differentiation, a dynamic change in morphologies of n-iPSCs-TMCs and p-iPSCs-TMCs was observed under the light microscope. Cells of the two groups gradually transitioned from their original clone morphology to a hexagonal shape. (a–d) Morphological changes of n-iPSCs-TMCs at different time points. (e–h) Morphological changes of p-iPSCs-TMCs at different time points. (h) Arrows indicate the aggregated cells, and circles indicate the abnormal cell morphology. Scale bars, 100 µm. (B,C) IF staining results show the dynamic changes in iPSCs' markers and TMCs' markers of n-iPSCs-TMCs and p-iPSCs-TMCs. The expression of iPSC markers (OCT4 and SOX2) gradually disappeared. Scale bars, 100 µm. n-iPSCs-TMCs, healthy individual-specific induced pluripotent stem cells-derived trabecular meshwork cells; p-iPSCs-TMCs, patient-specific induced pluripotent stem cells-derived trabecular meshwork cells; MYOC, Myocilin; VCAM1, Vascular Cell Adhesion Molecule 1; OCT4, Octamer-Binding Transcription Factor 4; SOX2, SRY-Box Transcription Factor 2.

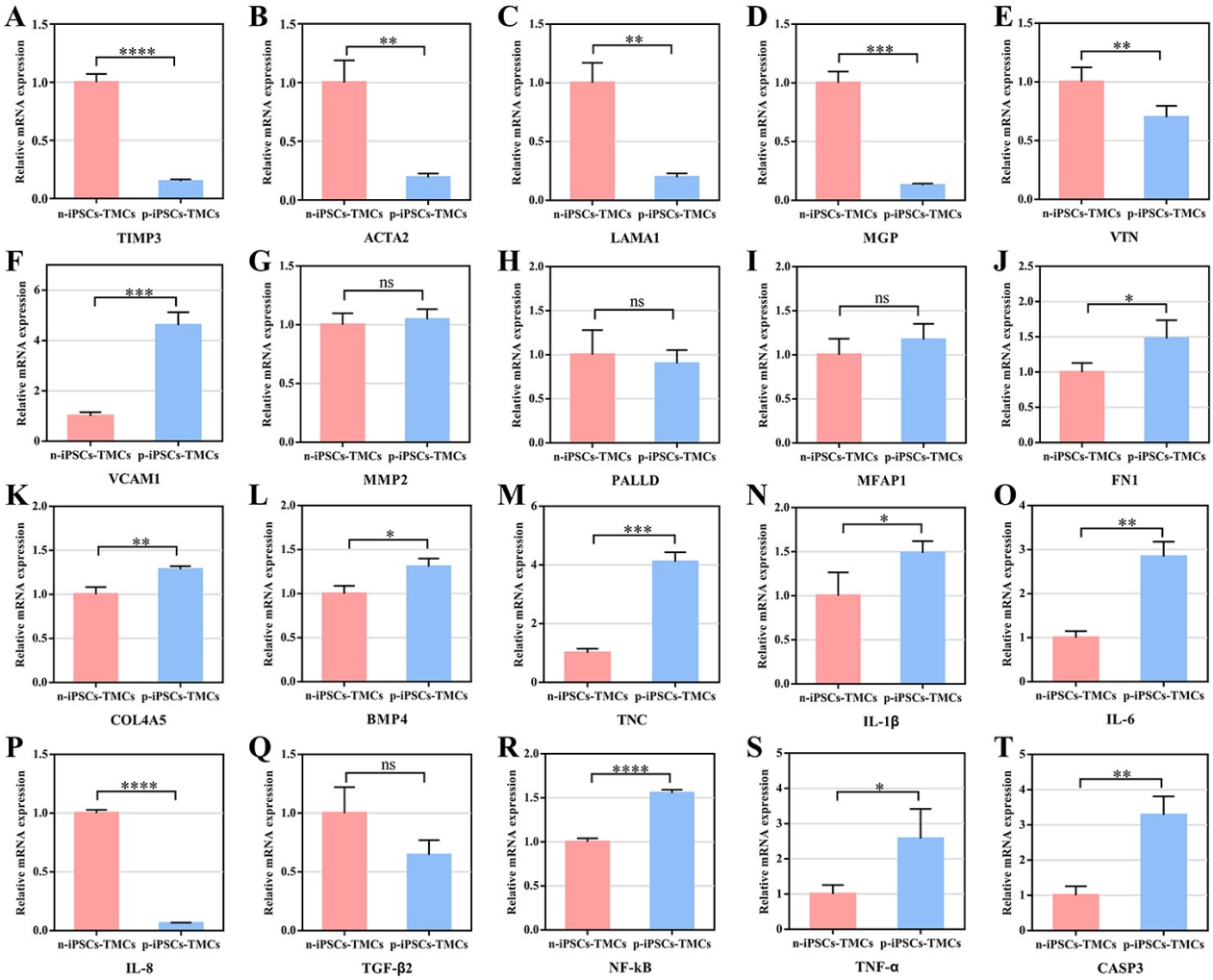

Fig. 3. The qRT-PCR results of two groups. The mRNA expression of *TIMP3* (A), *ACTA2* (B), *LAMA1* (C), *MGP* (D), and *VTN* (E) was downregulated in p-iPSCs-TMCs, while the mRNA expression of *VCAM1* (F), *FN1* (J), *COL4A5* (K), *BMP4* (L), *TNC* (M), *IL-1β* (N), Interleukin 6 (*IL-6*) (O), Interleukin 8 (*IL-8*) (P), *NF-κB* (R), *TNF-α* (S), and *CASP3* (T) were upregulated in them. The mRNA expression of *MMP2* (G), *PALLD* (H), *MFAP1* (I), and *TGF-β2* (Q) in the two groups was not significantly different. The error bars are mean plus standard deviation, n = 3, ****$p < 0.0001$; ***$p < 0.001$; **$p < 0.01$; *$p < 0.05$. "ns" represents the difference that is not statistically significant ($p > 0.05$).

450 nm was conducted utilizing a microplate reader (Bio-Tek, Burlington, VT, USA). The wells containing CCK-8 solution devoid of cells were used as a control to account for any background effects. Each experiment was conducted in triplicate, with triplicate wells included in each iteration.

Detection of Reactive Oxygen Species (ROS)

ROS in cells was detected using a ROS assay kit (Beyotime Biotechnology, #S0033S, Shanghai, China). Cells (10^4 per well) were seeded in a 96-well plate. 2′,7′-Dichlorodihydrofluorescein diacetate (DCFH-DA) and Dulbecco's Modified Eagle Medium (DMEM) media (Thermo Fisher Scientific, #11965092, Waltham, MA, USA) were mixed in a 1:1000 ratio and 100 microliters of the mixture was added to each well and incubated at 37 °C for 30 minutes. Then, the cells were washed with DMEM media three times gently. Fluorescence images were obtained. The fluorescence intensity of 2′,7′-dichlorofluorescein (DCF), denoting intracellular ROS generation, was evaluated using a multimode microplate reader (Bio-Tek, Burlington, VT, USA). 353 nm (Excitation wavelength) and 465 nm (Emission wavelength) were used for the DAPI channel, 493 nm (Excitation wavelength) and 517 nm (Emission wavelength) were used for the green channel. The assay was repeated in triplicate independently. According to the kit's instructions, DCFH-DA itself is non-fluorescent. When it enters the cell, it will be hydrolyzed by intracellular esterase to produce dichlorodihydrofluorescein (DCFH), and intracellular ROS can oxidize the non-fluorescent DCFH to produce flu-

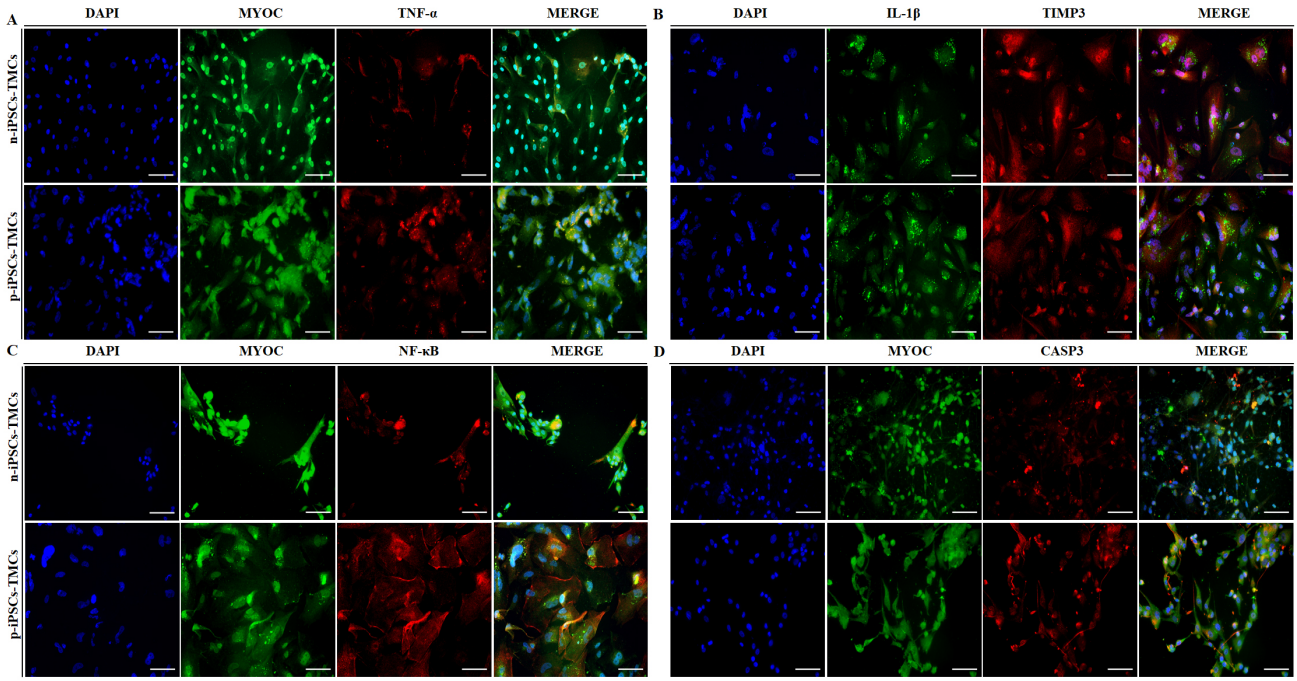

Fig. 4. The IF staining results of apoptosis and inflammatory markers in n-iPSCs-TMCs and p-iPSCs-TMCs. (A,B) TNF-α, IL-1β are positively expressed in two groups of cells. (C,D) NF-κB, and CASP3 are positively expressed in two groups of cells. MYOC and TIMP3 are used as the cell markers of n-iPSCs-TMCs and p-iPSCs-TMCs. Scale bars, 100 µm. TNF-α, Tumor Necrosis Factor-alpha; IL-1β, Interleukin 1 Beta; NF-κB, Nuclear Factor Kappa B; CASP3, Caspase 3; MYOC, Myocilin; TIMP3, TIMP metallopeptidase inhibitor 3; DAPI, 4′,6-Diamidino-2-phenylindole.

orescent DCF. By detecting the fluorescence intensity of DCF, we can know the level of intracellular ROS. Therefore, reagents that are not well mixed will not fluoresce. When a large amount of ROS is produced in the cell, it may lead to apoptosis, leaving dead cells suspended in the culture medium. In this experiment, we observed a few dotted or bright green highly fluorescent clusters under the fluorescence microscope, which we believe to be cellular debris or aggregates of dead cells suspended in the culture medium rather than impurities. This is an important component of ROS produced intracellular, so we retained them when obtaining images and detecting the fluorescence intensity.

Phagocytosis Assay

Cell phagocytosis was analyzed using a phagocytosis assay kit (Invitrogen, #P35366, Carlsbad, CA, USA) according to the manufacturer's instructions. pHrodo Green *E. coli* BioParticles were resuspended in Live Cell Imaging Solution (Thermo Fisher Scientific, #A59688DJ, Waltham, MA, USA) at 1 mg/mL. The cell medium was replaced with fresh Live Cell Imaging Solution (100 µL per well), and 10 µL of mixed bioparticles was added to each well. Then, the plate was incubated at 37 °C for three hours. After washed three times and stained with Hoechst 33342 Staining Solution for Live Cells (100×, Beyotime Biotechnology, #C1025, Shanghai, China) for ten minutes, the cells were bathed in the Live Imaging Solution. The results were evaluated using a multimode microplate reader (Bio-Tek, Burlington, VT, USA). 353 nm (Excitation wavelength) and 465 nm (Emission wavelength) were used for the Hoechst 33342 channel, 493 nm (Excitation wavelength), and 517 nm (Emission wavelength) were used for the green channel. The assay was repeated in triplicate independently. Fluorescence images were obtained. According to the kit instructions, *E. coli* particles are non-fluorescent and only fluoresce after being phagocytosed into the cell. In this experiment, we observed some dotted or green highly fluorescent clusters outside the cell under the microscope. We believe this is the fluorescence produced by the massive overflow of particles caused by apoptosis and cell membrane rupture of some dying cells after phagocytosis of *E. coli* particles. This is a real manifestation and direct evidence of the phagocytic state of the cells, so we retained them in the image acquisition and detection of the fluorescence intensity.

Statistical Analysis

A comparison between the two groups was performed using two-tailed Student's *t*-tests. A p-value < 0.05 was considered statistically significant. SPSS 17.0 (IBM Corp., Chicago, IL, USA) and GraphPad Prism 7 (GraphPad Software, Inc., San Diego, CA, USA) were used to perform the statistical analysis.

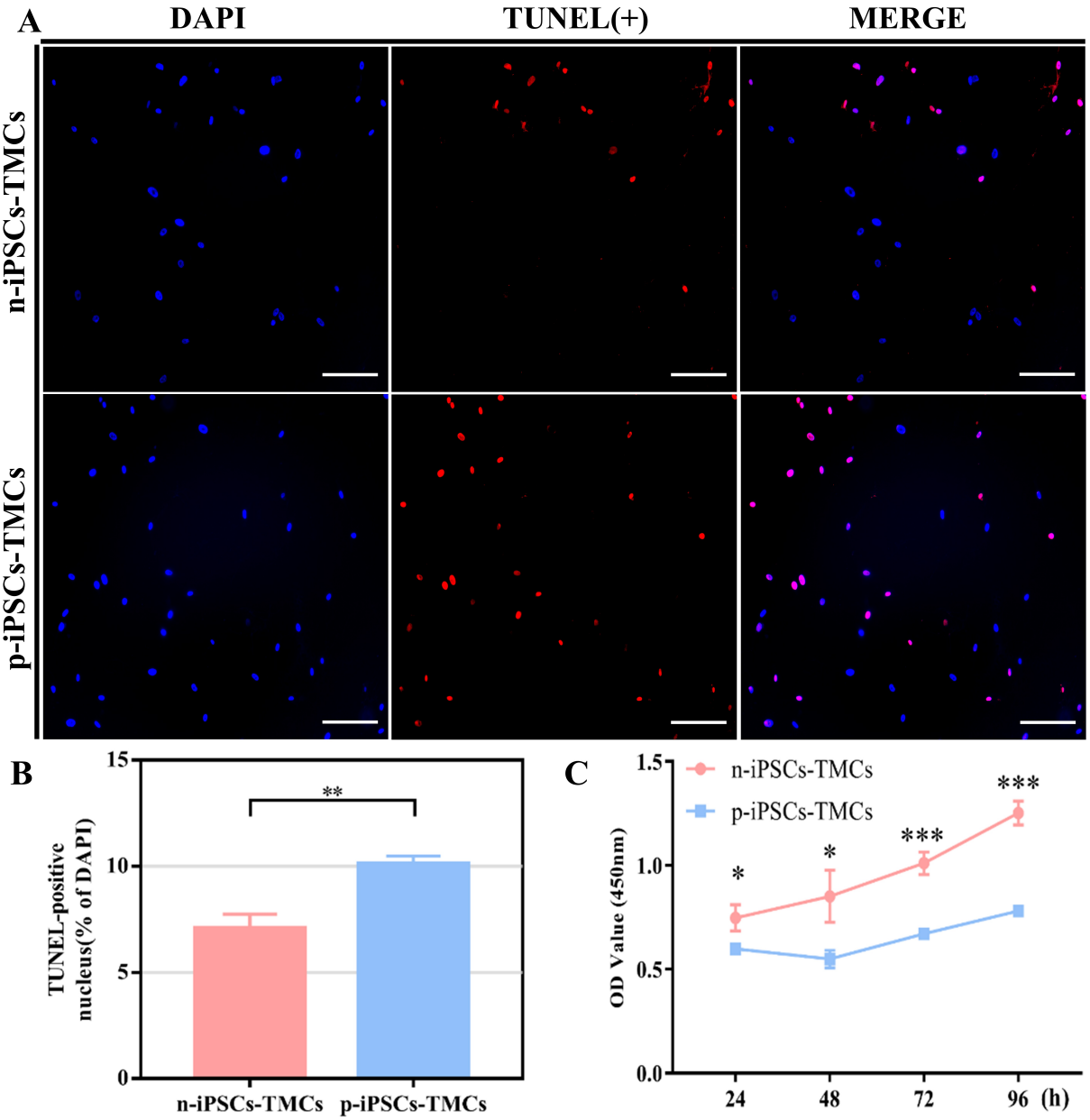

Fig. 5. TUNEL and CCK-8 results. (A,B) TUNEL results. (A) The result of TUNEL positive staining of cells in two groups. (B) Quantitative comparison of TUNEL-positive cells' number in two groups shows p-iPSCs-TMCs exhibit greater cell apoptosis ($p < 0.01$). (C) CCK-8 result. p-iPSCs-TMCs show impaired proliferating ability at all time points, compared with n-iPSCs-TMCs (24-h and 48-h time points: $p < 0.05$, 72-h and 96-h time points: $p < 0.001$). Scale bars, 100 µm. The error bars are mean plus standard deviation, n = 3, *$p < 0.05$, **$p < 0.01$, ***$p < 0.001$. TUNEL, Terminal Deoxynucleotidyl Transferase-Mediated dUTP Nick-End Labeling; CCK-8, Cell Counting Kit-8. "+" represents the positive of TUNEL cells.

Results

The Morphology of p-iPSCs was the Same as that of n-iPSCs

Twenty-one to twenty-eight days after the reprogramming and induction, the iPSC clones were observed. Under the light microscope, the morphology of p-iPSCs appeared similar to that of the n-iPSCs. The results of IF staining of the pluripotent markers TRA1-81 and NANOG showed positive expression in both types of cells, confirming the successful generation of iPSCs (Fig. 1).

p-iPSCs-TMCs Exhibited Morphology and Function Defects

The results showed that p-iPSCs-TMCs exhibited compromised morphology and function compared to n-

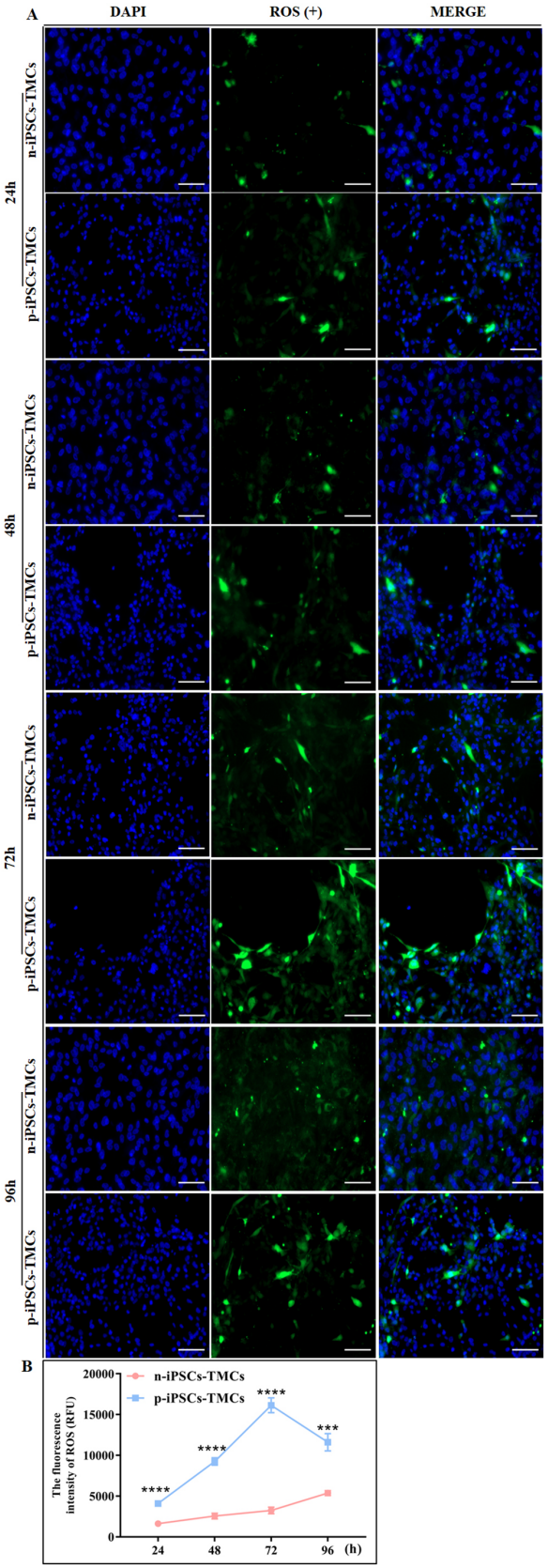

Fig. 6. ROS results. (A) The results of staining. ROS production is present in both groups of cells. (B) Quantitative comparisons of ROS show a higher total ROS production in p-iPSCs-TMCs than n-iPSCs-TMCs at any time point (24-h, 48-h, and 72-h time points: $p < 0.0001$, 96-h time point: $p < 0.001$). Scale bars, 100 µm. The error bars are mean plus standard deviation, n = 3, ****$p < 0.0001$; ***$p < 0.001$. ROS, reactive oxygen species. "+" represents the positive of ROS.

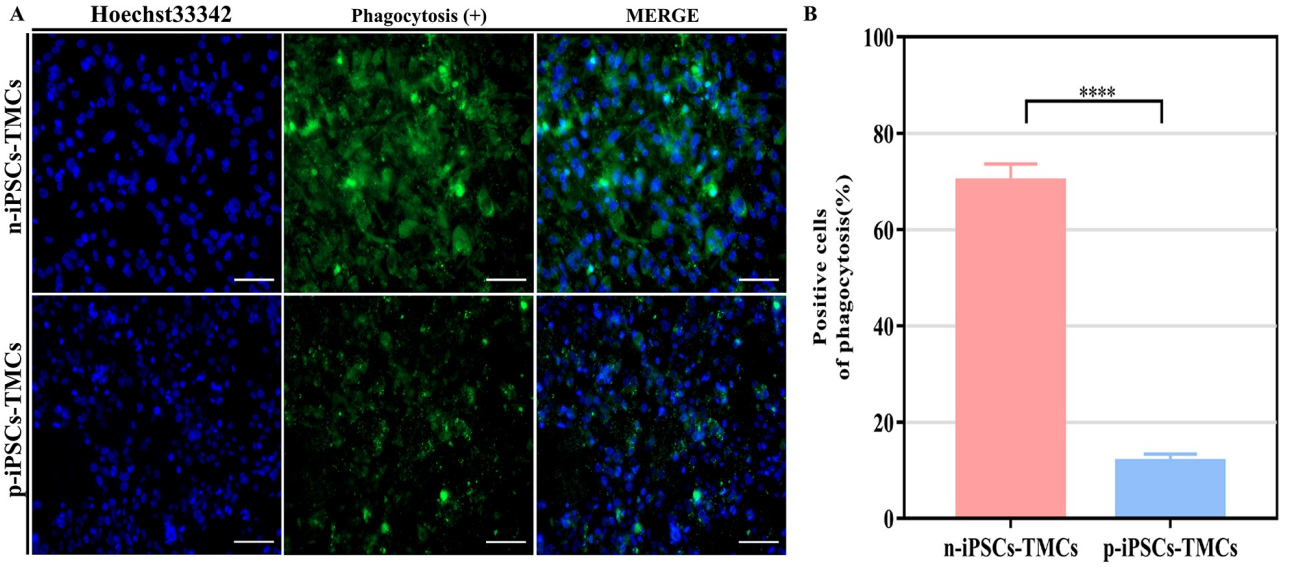

Fig. 7. The phagocytic capacity results. (A) The results of staining. (B) Quantitative comparison of ROS shows reduced phagocytosis in p-iPSCs-TMCs ($p < 0.0001$). Scale bars, 100 µm. The error bars are mean plus standard deviation, n = 3, ****$p < 0.0001$. "+" represents the positive of phagocytosis.

iPSCs-TMCs. Differentiation of iPSCs into iPSCs-TMCs began within the first week, typically within one to two days of induction. Over time, some iPSCs gradually transitioned from their original clone morphology to a hexagonal shape. In the following weeks, the number of circular iPSC-like cells gradually decreased, while the number of spindle-shaped cells gradually increased. The cells became dispersed. By the fourth week, more than 90% of TMC-like cells were observed (Fig. 2A). However, after four weeks of induction, p-iPSCs-TMCs had localized aggregates (shown by arrows) and unequal cell morphology in size (indicated by circles) (Fig. 2A,h), while n-iPSCs-TMCs showed a uniformly distributed and homogenous appearance (Fig. 2A,d). The IF staining results showed positive expression of the pluripotency markers OCT4 and SOX2 as well as the TMC markers MYOC and VCAM1 in the first week. As differentiation progressed, the expression of iPSC markers gradually disappeared. By the end of the fourth week, the majority of the iPSCs (>90%) had fully differentiated into iPSCs-TMCs, which no longer expressed OCT4 and SOX2 (Fig. 2B,C).

To identify the genes involved in cytoskeletal proteins, basal membrane components, inflammation, cell apoptosis, and ECM in the two groups, qRT-PCR was performed. The mRNA expression of *TIMP3* (Fig. 3A, $p < 0.0001$), *ACTA2* (Fig. 3B, $p < 0.01$), Laminin Subunit Alpha 1 (*LAMA1*) (Fig. 3C, $p < 0.01$), Matrix Gla Protein (*MGP*) (Fig. 3D, $p < 0.001$), and Vitronectin (*VTN*) (Fig. 3E, $p < 0.01$) was downregulated in p-iPSCs-TMCs, while the mRNA expression of *VCAM1* (Fig. 3F, $p < 0.001$), Fibronectin 1 (*FN1*) (Fig. 3J, $p < 0.05$), Collagen Type IV Alpha 5 (*COL4A5*) (Fig. 3K, $p < 0.01$), Bone Morphogenetic Protein 4 (*BMP4*) (Fig. 3L, $p < 0.05$), Tenascin C (*TNC*) (Fig. 3M, $p < 0.001$), *IL-1*β (Fig. 3N, $p < 0.05$), *IL-6* (Fig. 3O, $p < 0.01$), *IL-8* (Fig. 3P, $p < 0.0001$), *NF-*κ*B* (Fig. 3R, $p < 0.0001$), *TNF-*α (Fig. 3S, $p < 0.05$), and *CASP3* (Fig. 3T, $p < 0.01$) were upregulated in them. The mRNA expression of Matrix Metallopeptidase 2 (*MMP2*) (Fig. 3G, $p > 0.05$), Palladin (*PALLD*) (Fig. 3H, $p > 0.05$), Microfibril Associated Protein 1 (*MFAP1*) (Fig. 3I, $p > 0.05$), and Transforming Growth Factor Beta 2 (TGF-β2) (Fig. 3Q, $p > 0.05$) in the two groups was not significantly different. The IF result showed positive expression of inflammation and cell apoptosis markers, such as TNF-α, IL-1β, NF-κB, and CASP3 in two groups of cells (Fig. 4). In addition, the results of TUNEL and CCK-8 suggested that compared with n-iPSCs-TMCs, p-iPSCs-TMCs showed increased cell apoptosis (Fig. 5A,B) ($p < 0.01$) and decreased proliferation ability (Fig. 5C) (24-h and 48-h time points: $p < 0.05$, 72-h and 96-h time points: $p < 0.001$). The ROS assay showed a higher level of oxidative stress in p-iPSCs-TMCs at different time points (24-h, 48-h, and 72-h time points: $p < 0.0001$, 96-h time point: $p < 0.001$) (Fig. 6). Furthermore, the phagocytosis ability of p-iPSCs-TMCs was impaired compared to that of n-iPSCs-TMCs ($p < 0.0001$) (Fig. 7).

Discussion

During the years of follow-up, we have observed significant differences in phenotypes among the patients, such as severe optic nerve damage and sagging thin-wall filtering blebs. With the increase in family members and patients, some members show discordance between genotype and phenotype. To explore the underlying mechanisms for these phenomena, we preliminarily constructed a POAG model

based on the iPSC technology. Since trabecular meshwork is a crucial target tissue for POAG attacks, iPSCs-TMCs were generated. iPSCs can be induced to differentiate into many needed cell types because of their pluripotency. Retinal ganglion cells and trabecular meshwork cells derived from iPSCs have been generated to date [14,20–22]. In addition, three-dimensional (3D) culture human trabecular meshwork cells (HTMCs) or retinal organoids have been constructed [7,8,10,23,24]. However, there are few reports about iPSCs-derived disease models for familial POAG. In the experiment, we successfully reprogrammed the PBCs of patients in GZ.1 into iPSCs and differentiated the cells into iPSCs-TMCs, establishing the solid groundwork for future research on pathogenesis and gene therapy.

In this research, we demonstrated that the cell marker expression of p-iPSCs-TMCs and n-iPSCs-TMCs closely resembled that of HTMCs. However, p-iPSCs-TMCs exhibited a more significantly heterogeneous appearance with varying sizes and clumped aggregation. At the same time, the n-iPSCs-TMCs displayed a uniform and homogeneous appearance similar to that of HTMCs. The decreased mRNA expression of cytoskeletal proteins, basal membrane components, and proteins secreted by p-iPSCs-TMCs, such as *VTN*1, *TIMP3*, *ACTA2*, and *LAMA1*, indicates a compromised capacity to maintain morphology and function.

In addition, elevated IOP is the main factor contributing to POAG. A shred of compelling evidence [25,26] has shown that excessive ECM deposition and calcification in the trabecular meshwork (TM) play an important role in fibrosis and distortion of the TM framework, leading to increased resistance to aqueous humor outflow and elevation of IOP. Upregulation of ECM components in p-iPSCs-TMCs, such as *FN1* [27], *COL4A5* [27], *VCAM1* [28], and *TNC* [15], was observed in our study, which may enhance cellular stiffness and lead to increased fibrosis and resistance compared to n-iPSCs-TMCs. Moreover, the results showed the downregulation of *MGP* in p-iPSCs-TMCs. It is known that *MGP* encodes the protein of the osteocalcin/matrix Gla family, which functions as a physiological inhibitor of tissue calcification [29–32]. Therefore, we hypothesize that the downregulated expression of *MGP* might contribute to p-iPSCs-TMCs abnormalities. Additionally, the current view holds that apoptosis, oxidative stress, and inflammation are associated with POAG [33,34]. The increased mRNA expression of *IL-1*β, *IL-6*, *TNF-*α, *NF-*κ*B*, and *CASP3* in p-iPSCs-TMCs indicated the activation of apoptosis and inflammatory signaling pathways. This finding was also validated by the IF staining, CCK-8, TUNEL, and ROS assays. Notably, the generation of ROS in the p-iPSCs-TMCs group decreased 96 hours later, while that in the n-iPSCs-TMCs group didn't. We believe that the higher level of ROS in the two p-iPSCs-TMCs group compared to the n-iPSCs-TMCs group resulted in more severe intracellular oxidative stress. The intracellular ROS content peaked after 72 hours, leading to increased apoptosis and ultimately decreased number of cells and the fluorescence intensities in the p-iPSCs-TMCs group after 96 hours. Although the fluorescence measured was lower, the overall level of ROS content was significantly higher in the p-iPSCs-TMCs group than in the n-iPSCs-TMCs group, with a statistically significant difference. Furthermore, the phagocytosis experiment demonstrated that p-iPSCs-TMCs displayed a diminished capacity to effectively eliminate metabolites, potentially obstructing the trabecular meshwork and resulting in an elevation in IOP. In summary, p-iPSCs-TMCs exhibit a strong tendency to excessive ECM deposition, calcification, and fibrosis, in addition to heightened levels of cell apoptosis and ROS production and impaired phagocytic capabilities compared to n-iPSCs-TMCs.

Conclusion

This study successfully induced p-iPSCs and n-iPSCs into iPSCs-TMCs, which preliminarily constructed a POAG model in GZ.1. In addition, the research on the morphology and function of iPSCs-TMCs may be valuable for our understanding of pathogenesis and phenotypic differences in this family. This experiment is an initial exploration of p-iPSCs-TMCs. Flow cytometry is a more accurate method for detecting apoptosis. In the following study, we will perform this experiment to determine the survival status of cells and establish 3D cultures of the human trabecular meshwork in GZ.1 to perform more functional study. Gene sequencing and clustered regularly interspaced short palindromic repeats (CRISPR–Cas9) technology will be applied to pathogenic mechanism studies and alternative treatments.

Availability of Data and Materials

The data used or analyzed during the study are available from the corresponding author upon reasonable request.

Author Contributions

HFR, ZML, MJT, JQT, ZGF, NNS, and JG designed the research study; HFR, ZML, and JQT performed the research; HFR, ZML, KJL, JQT, and RCY collected and analyzed the data. HFR and JG have been involved in drafting the manuscript and all authors have been involved in revising it critically for important intellectual content. All authors have given the final approval of the version to be published. All authors have participated sufficiently in the work to take public responsibility for appropriate portions of the content and agreed to be accountable for all aspects of the work in ensuring that questions related to its accuracy or integrity.

Ethics Approval and Consent to Participate

This study complies with the Declaration of Helsinki and was approved by the Human Research Ethics Committee of Zhongshan Ophthalmic Center, Sun Yat-sen University (Guangzhou, China) (Number: 2017KYPJ007, Date: 13 February 2017). Our experiments received the understanding and written consent of each participant.

Acknowledgment

We thank all the individuals of the GZ.1 who participated in this study. We also thank Professor Jing Zhuang for her valuable advice on experimental design. We thank all the groups who provided help in the process of our experiment.

Funding

This study was supported by the National Natural Science Foundation of China (grant number 81430009); the Science and Technology Planning Projects of Guangdong Province (grant number 2014B020225001, 2014B030301040, and 2017B030314025); and the National Key R&D Program of China (grant number 2018YFA0108300).

Conflict of Interest

The authors declare no conflict of interest.

Supplementary Material

Supplementary material associated with this article can be found, in the online version, at https://doi.org/10.24976/Discov.Med.202436189.185.

References

[1] Tham YC, Li X, Wong TY, Quigley HA, Aung T, Cheng CY. Global prevalence of glaucoma and projections of glaucoma burden through 2040: a systematic review and meta-analysis. Ophthalmology. 2014; 121: 2081–2090.

[2] Wiggs JL, Pasquale LR. Genetics of glaucoma. Human Molecular Genetics. 2017; 26: R21–R27.

[3] Lee JS, Kuo CF, Chen WM, Lin KK, See LC. Genetic and Environmental Contributions of Primary Angle-Closure Glaucoma and Primary Open-Angle Glaucoma: A Nationwide Study in Taiwan. American Journal of Ophthalmology. 2024; 258: 99–109.

[4] Gupta V, Somarajan BI, Gupta S, Chaurasia AK, Kumar S, Dutta P, *et al*. The inheritance of juvenile onset primary open angle glaucoma. Clinical Genetics. 2017; 92: 134–142.

[5] Sullivan MA, Lane SD, McKenzie ADJ, Ball SR, Sunde M, Neely GG, *et al*. iPSC-derived PSEN2 (N141I) astrocytes and microglia exhibit a primed inflammatory phenotype. Journal of Neuroinflammation. 2024; 21: 7.

[6] Verkerke M, Berdenis van Berlekom A, Donega V, Vonk D, Sluijs JA, Butt NF, *et al*. Transcriptomic and morphological maturation of human astrocytes in cerebral organoids. Glia. 2024; 72: 362–374.

[7] Hirami Y, Mandai M, Sugita S, Maeda A, Maeda T, Yamamoto M, *et al*. Safety and stable survival of stem-cell-derived retinal organoid for 2 years in patients with retinitis pigmentosa. Cell Stem Cell. 2023; 30: 1585–1596.e6.

[8] Lei Q, Xiang K, Cheng L, Xiang M. Human retinal organoids with an OPA1 mutation are defective in retinal ganglion cell differentiation and function. Stem Cell Reports. 2024; 19: 68–83.

[9] Penney J, Ralvenius WT, Loon A, Cerit O, Dileep V, Milo B, *et al*. iPSC-derived microglia carrying the TREM2 R47H/+ mutation are proinflammatory and promote synapse loss. Glia. 2024; 72: 452–469.

[10] Daniszewski M, Senabouth A, Liang HH, Han X, Lidgerwood GE, Hernández D, *et al*. Retinal ganglion cell-specific genetic regulation in primary open-angle glaucoma. Cell Genomics. 2022; 2: 100142.

[11] Zhuo YH, Wei YT, Bai YJ, Duan S, Lin MK, Saragovi HU, *et al*. Pro370Leu MYOC gene mutation in a large Chinese family with juvenile-onset open angle glaucoma: correlation between genotype and phenotype. Molecular Vision. 2008; 14: 1533–1539.

[12] Filla MS, Dimeo KD, Tong T, Peters DM. Disruption of fibronectin matrix affects type IV collagen, fibrillin and laminin deposition into extracellular matrix of human trabecular meshwork (HTM) cells. Experimental Eye Research. 2017; 165: 7–19.

[13] Tang B, Li S, Cao W, Sun X. The Association of Oxidative Stress Status with Open-Angle Glaucoma and Exfoliation Glaucoma: A Systematic Review and Meta-Analysis. Journal of Ophthalmology. 2019; 2019: 1803619.

[14] Ding QJ, Zhu W, Cook AC, Anfinson KR, Tucker BA, Kuehn MH. Induction of trabecular meshwork cells from induced pluripotent stem cells. Investigative Ophthalmology & Visual Science. 2014; 55: 7065–7072.

[15] Keller KE, Kelley MJ, Acott TS. Extracellular matrix gene alternative splicing by trabecular meshwork cells in response to mechanical stretching. Investigative Ophthalmology & Visual Science. 2007; 48: 1164–1172.

[16] Loh YH, Agarwal S, Park IH, Urbach A, Huo H, Heffner GC, *et al*. Generation of induced pluripotent stem cells from human blood. Blood. 2009; 113: 5476–5479.

[17] Zhou H, Martinez H, Sun B, Li A, Zimmer M, Katsanis N, *et al*. Rapid and Efficient Generation of Transgene-Free iPSC from a Small Volume of Cryopreserved Blood. Stem Cell Reviews and Reports. 2015; 11: 652–665.

[18] Zeng J, Tang SY, Toh LL, Wang S. Generation of "Off-the-Shelf" Natural Killer Cells from Peripheral Blood Cell-Derived Induced Pluripotent Stem Cells. Stem Cell Reports. 2017; 9: 1796–1812.

[19] Deng F, Hu H, Chen M, Sun X, Liu X, Dong Z, *et al*. Generation of induced pluripotent stem cells from human Tenon's capsule fibroblasts. Molecular Vision. 2012; 18: 2871–2881.

[20] Zhong X, Gutierrez C, Xue T, Hampton C, Vergara MN, Cao LH, *et al*. Generation of three-dimensional retinal tissue with functional photoreceptors from human iPSCs. Nature Communications. 2014; 5: 4047.

[21] Li K, Zhong X, Yang S, Luo Z, Li K, Liu Y, *et al*. HiPSC-derived retinal ganglion cells grow dendritic arbors and functional axons on a tissue-engineered scaffold. Acta Biomaterialia. 2017; 54: 117–127.

[22] Feng P, Wang W, Xu W, Cao Q, Zhu W. Application of a Magnetic Platform in α6 Integrin-Positive iPSC-TM Purification. Bioengineering (Basel, Switzerland). 2023; 10: 410.

[23] Tian YI, Zhang X, Torrejon K, Danias J, Du Y, Xie Y. A Biomimetic, Stem Cell-Derived In Vitro Ocular Outflow Model. Advanced Biosystems. 2020; 4: e2000004.

[24] Qu Z, Batz Z, Singh N, Marchal C, Swaroop A. Stage-specific dynamic reorganization of genome topology shapes transcriptional neighborhoods in developing human retinal organoids. Cell Reports. 2023; 42: 113543.

[25] Stamer WD, Acott TS. Current understanding of conventional outflow dysfunction in glaucoma. Current Opinion in Ophthalmology. 2012; 23: 135–143.

[26] Pattabiraman PP, Toris CB. The exit strategy: Pharmacological modulation of extracellular matrix production and deposition for better aqueous humor drainage. European Journal of Pharmacology. 2016; 787: 32–42.

[27] Tawara A, Tou N, Kubota T, Harada Y, Yokota K. Immunohistochemical evaluation of the extracellular matrix in trabecular meshwork in steroid-induced glaucoma. Graefe's Archive for Clinical and Experimental Ophthalmology. 2008; 246: 1021–1028.

[28] Gharahkhani P, Jorgenson E, Hysi P, Khawaja AP, Pendergrass S, Han X, *et al*. Genome-wide meta-analysis identifies 127 open-angle glaucoma loci with consistent effect across ancestries. Nature Communications. 2021; 12: 1258.

[29] Borrás T, Cowley DO, Asokan P, Pandya K. Generation of a Matrix Gla (Mgp) floxed mouse, followed by conditional knockout, uncovers a new Mgp function in the eye. Scientific Reports. 2020; 10: 18583.

[30] Borrás T, Smith MH, Buie LK. A Novel Mgp-Cre Knock-In Mouse Reveals an Anticalcification/Antistiffness Candidate Gene in the Trabecular Meshwork and Peripapillary Scleral Region. Investigative Ophthalmology & Visual Science. 2015; 56: 2203–2214.

[31] Khavandgar Z, Roman H, Li J, Lee S, Vali H, Brinckmann J, *et al*. Elastin haploinsufficiency impedes the progression of arterial calcification in MGP-deficient mice. Journal of Bone and Mineral Research: the Official Journal of the American Society for Bone and Mineral Research. 2014; 29: 327–337.

[32] Malhotra R, Nicholson CJ, Wang D, Bhambhani V, Paniagua S, Slocum C, *et al*. Matrix Gla Protein Levels Are Associated With Arterial Stiffness and Incident Heart Failure With Preserved Ejection Fraction. Arteriosclerosis, Thrombosis, and Vascular Biology. 2022; 42: e61–e73.

[33] Vernazza S, Tirendi S, Passalacqua M, Piacente F, Scarfì S, Oddone F, *et al*. An Innovative In Vitro Open-Angle Glaucoma Model (IVOM) Shows Changes Induced by Increased Ocular Pressure and Oxidative Stress. International Journal of Molecular Sciences. 2021; 22: 12129.

[34] Raga-Cervera J, Bolarin JM, Millan JM, Garcia-Medina JJ, Pedrola L, Abellán-Abenza J, *et al*. miRNAs and Genes Involved in the Interplay between Ocular Hypertension and Primary Open-Angle Glaucoma. Oxidative Stress, Inflammation, and Apoptosis Networks. Journal of Clinical Medicine. 2021; 10: 2227.